

FACILITY FORM 602

**N67 12988**  
(ACCESSION NUMBER)  
**35**  
(PAGES)  
**CR 80362**  
(NASA CR OR TMX OR AD NUMBER)

\_\_\_\_\_  
(THRU)  
 \_\_\_\_\_  
(CODE)  
**12**  
(CATEGORY)

GPO PRICE \$ \_\_\_\_\_

CFSTI PRICE(S) \$ \_\_\_\_\_

Hard copy (HC) 2.00

Microfiche (MF) .50

# 653 July 65



**WYLE LABORATORIES**  
 TESTING DIVISION, HUNTSVILLE FACILITY

research

WYLE LABORATORIES - RESEARCH STAFF  
REPORT NUMBER WR 66-44

SOME SHADOWGRAPH EXPERIMENTS  
WITH A COLD, SUPERSONIC JET

This Report was Completed Under Contract NAS8-11312

Prepared by

*J. Offerhead*  
J. Offerhead

Approved by

*R. C. Potter*  
R. C. Potter  
Program Manager

Approved by

*L. C. Sutherland*  
L. C. Sutherland  
Research Operations Manager

Date October 1966

4

COPY NO. \_\_\_\_\_



## SUMMARY

A series of shadowgraphs are presented which show the flow structure and acoustic radiation of a small, cold, supersonic jet. The position of the film is shown to have a significant effect upon the nature of the photographic image but experiments, attempting to "focus" the shadowgraph by means of lenses, are inconclusive.

Acoustic wave radiation which is visible in the shadowgraphs takes two distinct forms. The first is a highly directional radiation, generated in a region near the nozzle, whose origin is uncertain but which is tentatively associated with "Mach Waves". The second is spherical in nature and originates from a series of highly localized regions in the exhaust stream. These sources are traced to the intersections of standing compression shocks in the flow with supersonically convected turbulence.

## ACKNOWLEDGEMENT

Many thanks are due to Dr. M. V. Lowson for his considerable assistance with the experimental work and for many helpful comments.

## TABLE OF CONTENTS

	<u>Page Number</u>
SUMMARY	ii
ACKNOWLEDGEMENT	iii
TABLE OF CONTENTS	iv
LIST OF FIGURES	v
1.0 INTRODUCTION	1
2.0 EXPERIMENTAL APPARATUS	2
2.1 Nitrogen Supply	2
2.2 Test Rig	2
2.3 Optical Apparatus	3
2.4 Procedure	3
3.0 RESULTS	4
3.1 Optical Experiments	4
3.2 The Acoustic Field of the Jet Exhaust Stream	6
4.0 CONCLUSIONS AND RECOMMENDATIONS	13
REFERENCES	15
FIGURES	16-21
PLATES 1-9	22-30

## LIST OF FIGURES

<u>Figure Number</u>		<u>Page Number</u>
1	Experimental Apparatus	16
2	Model Jet - Convergent/Divergent Nozzle	17
3	Variation of Nozzle Exit Velocity (Expressed as Mach Number Relative to Ambient Speed of Sound) With Nitrogen Storage Pressure	17
4	Regions of Apparent Locations of Multidirectional Sound Sources	18
5	Idealized Representation of Flow Structure Showing Acoustic Source Location	19
6a	Sound Ray Refraction	20
6b	Center of Curvature of Transmitted Waves	20
7	Wave Propagation and Radiation From a Stationary Simple Source Immersed at Unit Depth in a Fluid Moving with Sonic Velocity	21

## 1.0 INTRODUCTION

As part of the continued study of the noise generating mechanisms of rocket exhaust flow, a series of shadowgraph experiments have been planned and are currently being executed in the Marshall Space Flight Center jet flow facilities (Reference 1). In the nature of a preliminary exploratory investigation to support this work, Wyle Laboratories have conducted some similar tests using a small Mach 2.5 nitrogen jet, to examine the potentialities of the shadowgraph technique for the study of the acoustic and turbulence properties of jet flow. The basic objective of these experiments was to examine both the effects of varying the film position and the focusing effects of lenses. The high speed spark source used for this work was built to a design by Marshall Space Flight Center and it is due to the excellent performance of this device and to the previous experience of both Marshall Space Flight Center and Langley Research Center in the use of film, that no difficulty was encountered in producing shadowgraphs of good quality.

It was found that varying the jet-to-film distance had a significant effect upon the image character of both the turbulent flow and the acoustic field and it is concluded that careful consideration must be given to both the optical layout and shadowgraph interpretation in future work.

The use of lenses in the optical system, on the other hand, remains inconclusive at the present time. It was believed that a diverging lens might be utilized to bring different regions of the turbulent flow into focus but the present results suggest that its only effect is to produce an image magnification, similar to that which might be expected by increasing the film distance.

In addition to meeting the basic objectives, the experiments shed a little more light onto the basic problem of rocket exhaust noise generation as well as posing a few more questions. Although the jet velocity was estimated to be only approximately 1.25 times the ambient atmospheric speed of sound, clear evidence was obtained of both highly directional sound radiation from a region near the nozzle lip, tentatively associated with "Mach Waves", and a spherical type of radiation from a series of discrete locations in the flow, believed to be the result of shock/turbulence interaction. An explanation is put forward for the apparent location of these sources.

## 2.0 EXPERIMENTAL APPARATUS

### 2.1 Nitrogen Supply

Nitrogen was chosen as a working fluid simply because of its abundant high pressure supply at Wyle. Six manifolded bottles are available, holding a total of 150 cu.ft. of gaseous nitrogen at 2,200 psi. This is sufficient for more than 30 minutes continuous running of the model jet. Also, the bottles can be recharged from a liquid nitrogen storage tank.

### 2.2 Test Rig

The model jet rig was assembled on a granite surface table, chosen for the convenience of the optical experiments. A schematic of the layout is shown in Figure 1. The nozzle was mounted, with its axis horizontal, roughly 12 inches from the surface. The high pressure gas supply was reduced to the working pressure through a dome regulator and supplied to the nozzle through a one inch diameter steel pipe. A shut off valve enabled the pressure control to remain set during any series of runs, and a 300 psig safety valve was installed between the valve and the regulator. A pressure gauge measured the static pressure in the one inch nozzle supply pipe, downstream of the shut off valve. Since the flow velocity in this pipe was less than 100 ft./sec., the dynamic pressure error is negligible.

The converging-diverging nozzle is shown in Figure 2. It has a one centimeter diameter orifice and a design exit Mach number of 2.5. The expansion contours were designed on the basis of the one-dimensional flow relationships of Reference 2 with the intention of preserving continuity of the flow properties from the throat to the exit plane. However, as will be seen from the shadowgraphs, the severe shock structure in the flow, at design point operation, indicates that the expansion is far from ideal, probably due to a combination of the inadequacy of one-dimensional theory and imperfections of manufacture. The nozzle was machined from aluminum alloy and was found difficult to achieve a perfectly smooth inside surface because of its small size.

The theoretical performance of the nozzle is as follows:

Design pressure ratio	$P_0/P_E$	=	17.1	{ Where suffix 0 denotes nozzle supply conditions. E denotes exit plane conditions.
Exit Mach Number	$M_E$	=	2.50	
Temperature ratio	$T_0/T_E$	=	2.25	

Thus for an atmospheric pressure of 14.7 psia, the supply pressure required is 251 psia.

As a result of the very high storage pressure of around 2,000 psi, the temperature of the exhaust gas is extremely low. For this storage pressure, an ambient pressure of 14.7 psia, and a completely adiabatic expansion throughout the system, the theoretical exhaust temperature is approximately -330 degrees Fahrenheit. Thus, although the exit flow Mach number is 2.5, because of the low temperature and the consequent low speed of sound in the exhaust gas, the actual exhaust velocity is a much smaller multiple of the ambient speed of sound. For the example quoted, the theoretical jet velocity is approximately 1,390 feet per second. A much more meaningful velocity parameter, from an acoustic standpoint, is the effective jet Mach number  $M_E$ , defined as the ratio of jet velocity to the ambient speed of sound. This is a function of temperature, which varies with storage pressure, and Figure 3 shows the theoretical variation of  $M_E$  with storage pressure. It is seen to fall from a value of 1.5 at 480 psig to 1.22 at 2,200 psig.

The actual exhaust velocity achieved is probably higher than the theoretical value, since the expansions through both the regulator and nozzle will not be perfectly isentropic. With the intention of measuring the temperature of the supply gas, from which to estimate the actual exhaust velocity, a thermocouple was installed in the supply pipe adjacent to the pressure gauge. Unfortunately, it was discovered during the experiments that the thermocouple had malfunctioned and the temperature measurements were worthless.

## 2.3 Optical Apparatus

The basic components of an optical system for shadowgraphy are a spark source and a sheet of photographic film. A complete spark source unit, including a power supply, was loaned by Marshall Space Flight Center. This source is claimed to have a spark duration of less than one microsecond. For all tests conducted, the spark was located 137 centimeters from the nozzle center. The film used was 4" x 5" Kodak Royal Pan. This is a very fast (400 ASA) panchromatic film with moderate contrast, medium grain size, and a wide exposure and development latitude which had previously been used with success for shadowgraph work by Marshall Space Flight Center. The film was mounted in a standard film-pack on an optical bench carrier. The bench was aligned so that the film center could be moved along a line, normal to the jet axis, which passed through the spark and nozzle centers. For the focusing experiments, the lens was mounted in a holder on the same optical bench.

## 2.4 Procedure

It was found impossible to completely seal off all light from the laboratory and, although leakage was very small, precautions were taken to minimize interference from stray light. For each run, the optical configuration and gas pressure were set and the film pack was loaded. The lights were then extinguished and, in rapid succession, the following sequence of operations proceeded: open jet shut-off valve; open film pack; fire spark; close film pack; shut-off jet. This procedure minimized both film exposure to stray light and jet running time (desirable to prevent large variation of gas storage pressure during a series of runs).

### 3.0 RESULTS

#### 3.1 Optical Experiments

All the shadowgraphs, a representative selection of which are presented as plates 1 through 9, were made with the spark source located 137 centimeters from the jet axis. The main effect of spark distance is to regulate the illumination intensity at the film. However, since a shadowgraph registers the second rate of change of density, density gradients in a direction normal to the incident light ray are responsible for the predominant features of the image. Thus, a secondary effect of spark distance is to vary the plane of the projected density gradients. For parallel light, i.e., an infinite source distance, the projected plane is through the center of the jet and normal to the light beam. As spark distance is decreased, this plane is distorted to a curved surface, which is in fact the surface of a sphere having the light source as its center. For this reason it is desirable to keep the spark distance as large as possible. The particular source location in these experiments was selected to compromise illumination intensity and "image plane" distortion.

##### Plate 1 - Film Located 5 Centimeters From Jet Axis

The "diamond" shock pattern is clearly visible in the flow, with the compression shocks being particularly well defined. These shocks result primarily from the poor nozzle expansion but the flow divergence near the nozzle indicates that the flow is slightly under-expanded. There is some indication of an acoustic field, mainly evidenced as a highly directional radiation from a region near the nozzle. However, it is not very clear.

##### Plate 2 - Film Distance = 10 Centimeters

The turbulence scale is increased and the compression shocks appear to have lost some of their "sharpness". A dark fringe surrounding the initial portion of the flow which was insignificant in plate 1 is here clearly evident. This is a result of the cylindrical lens effect of the cold, dense jet stream; the beam of light which passes through the jet converges before reaching the film, leaving a non-illuminated gap. This effect is masked further downstream where density gradients are reduced.

The acoustic field shows more detail. The highly directional radiation is seen to originate from the flow upstream of the first compression shock and there is now some evidence of some multi-directional radiation emerging from locations downstream from the compression shocks.



Plate 3 - Film Distance = 20 Centimeters

The turbulence scale is further increased, and the shock fronts are becoming more vague. The acoustic field is more pronounced and the "spherical" radiation is quite clear. It can be seen to penetrate beyond the previous cut-off boundary associated with the directional radiation from near the nozzle.

Plate 4 - Film Distance = 50 Centimeters

The flow image shows significant extensions of the trends previously observed with increase of film distance. In particular, the turbulence scale is much larger and the dark fringe is extensive.

Plate 5 - Film Distance = 100 Centimeters

Here the film distance is almost as great as the spark distance and, although the acoustic field is still very pronounced and highly magnified, there is a marked lack of definition, probably due to the low level of illumination at this distance and the consequent excessive development required. Generally, the picture bears a striking resemblance to surface waves on a liquid.

Plate 6 - Film Distance = 200 Centimeters

The film distance is obviously too great in this instance. There is enormous magnification of the wave fronts but the area covered is too small and practically all definition is lost. A more intense spark would be required to produce useful shadowgraphs at this range.

Plates 7 and 8 -

Two inch diameter diverging lens of 20 centimeters focal length, located 10 centimeters from jet axis. Jet-to-film distance 20 centimeters (plate 7) and 30 centimeters (plate 8).

A comparison of these shadowgraphs and plate 3 (where the film was located 20 centimeters from the Jet) shows the basic difference to be in the size of the image. There is no significant difference in either the turbulence character or the acoustic field. An interesting feature which is extremely clear in plate 8 is the presence of "striations" which accompany compression and expansion waves in the flow. These were initially believed to be optical effects associated with the lens but a closer inspection of both plates 7 and 3 reveal the same structure. It is therefore, assumed to be a diffraction phenomenon connected with very large density gradients in the flow. Another diffraction pattern, this time circular, can be seen below the center of the lower compression shock in plate 8. This is probably due to a blemish in the lens or a dust particle.

### Plate 9 - Film Distance = 40 Centimeters

Converging lens of 100 centimeters focal length at 20 centimeters from jet.

Again the image is very similar to that of plate 3, this time showing a reduction in size. Distortions produced by the lens are apparent, particularly near its edges in the form of radial fringes.

## 3.2 The Acoustic Field of the Jet Exhaust Stream

The shadowgraphs (plates 1 through 6) show what appears to be two forms of acoustic radiation.

### Directional Radiation From Nozzle Region

The first of these which is most pronounced in plate 2, but which is clearly visible in plates 3 and 4 also, is a form of highly directional radiation emanating from the region in the close vicinity of the nozzle. The wave fronts show a slight curvature but the mean direction of propagation is inclined at approximately 47 degrees to the jet flow axis.

These waves are of the nature of "Mach Waves", first studied, and so named, by Phillips (Reference 3) and later investigated in greater detail by Ffowcs Williams (Reference 4). Mach waves can be thought of as weak shock waves associated with supersonically convected eddies (relative to the ambient speed of sound) in the jet mixing region and thus could well be expected to exhibit some curvature, since their generating eddies will move with an ever decreasing velocity during their lifetimes. Now supersonic eddies will be generated at least in the immediate boundary of the supersonic laminar core. However, mean velocities in the mixing region diminish with increasing distance from the nozzle as more mass flow is induced from the surrounding air, and the likelihood of generating supersonic moving eddies is therefore reduced with distance from the nozzle. Thus, a Mach wave field can be expected to be more intense towards the flow origin, an observed fact in this case, which therefore lends support to the supposition that these acoustic disturbances are in fact, Mach waves.

On the other hand, the direction of the radiation is puzzling. The mean propagation angle of 47 degrees to the flow direction implies an associated eddy convection Mach number of  $1.47 (= 1/\cos \theta)$  relative to the ambient speed of sound. This is actually greater than the estimated exhaust velocity of approximately  $M_E = 1.25$  and it is hardly likely that eddies are generated which travel faster than the mean flow. Ffowcs Williams has in fact suggested that significant noise producing eddies have convection velocities ranging between 0.2 and 0.7 times the mean flow velocity.

Two conclusions are possible. The first is that if the observed directional radiation is of the form of Mach waves, then the generating eddies are moving with velocities which are much closer to the jet nozzle velocity than has previously been supposed. The theoretical jet Mach number of  $M_E = 1.25$ , is based on isentropic expansion conditions and is quite probably underestimated, although it seems unlikely that the actual velocity would exceed  $M_E = 1.47$  by any significant margin. It is unfortunate that the temperature measurements, which would have confirmed this, were unsuccessful. Evidence which corroborates the finding that eddy velocities are apparently high, can be found in unpublished shadowgraphs (but see Reference 1) of a Mach 2.2 jet made by W. Mayes of the Langley Research Center. The Mach wave angle measured from these pictures corresponds to an eddy velocity which is again equal to the nozzle exhaust velocity.

The alternative conclusion is that the observed directional radiation field is not composed of Mach waves. A likely source of noise is that caused by the interaction of turbulent disturbances and a standing shock structure within the nozzle itself. Such disturbances could be generated upstream of the nozzle or within the nozzle boundary layer. Sound radiation from this source could well be expected to exhibit the sharp "cut-off" at some acute angle to the flow, in the same manner as that observed in the shadowgraphs.

#### Shock/Turbulence Noise

The second type of radiation, which becomes increasingly clear in plates 2 through 6, shows much less directionality and originates from a number of isolated regions in the flow. The sources are regularly spaced and Figure 4 shows a diagram of the jet structure on which has been superimposed the extent of these source regions. These were determined by close examination of the entire set of shadowgraphs and tracing the origin of any well defined wave segment, assumed to be an arc of a circle, to a point in the flow. The source boundaries show the envelopes of the strong concentrations of such "point sources". In fact, it is found that these sources extend from the regions shown, along a line normal to the axis, across the entire jet. It is believed that the latter is a three dimensional effect, this extended line in fact representing the side view of a "doughnut-shaped" source region. Figure 4 represents a normal slice through the jet showing what are believed to be the extent of the source locations in the vertical plane through the axis. It can be seen that these are related to the standing shock pattern in the flow.

Figure 5 shows a more complete picture of the flow structure. The flow can be divided into three regions: (a) a supersonic laminar core surrounded by (b) a conical region where the flow is still supersonic but turbulent and (c) a subsonic turbulent mixing region which is similar to that of a subsonic jet. The length of the laminar core (11.5 diameters) was obtained from the empirical relationship of Reference 5, and that of the supersonic core (22.5 diameters) from the experimental data of Reference 6. It is both interesting and significant that the portions of the

compression shocks which lie within the laminar core are precisely those portions which are visible in the shadowgraphs (plate 1). The shock fronts which penetrate the turbulent flow are obviously less well defined and do not form a clear image on the shadowgraph.

However, it appears likely that it is these latter portions of the compression shocks which lie within the turbulent flow which give rise to the localized sound sources; sound which is generated by the convection of turbulent eddies through the shock. the apparent shift of the source regions to areas which are displaced downstream and outwards from the shock/turbulence interaction positions are due to propagation and refraction of the sound before it reaches the ambient air.

The following explanation of this phenomenon utilizes a simplified physical model which retains the essential features of the real flow.

Consider a simple source immersed at unit depth in a fluid (1) which moves with velocity  $U$  parallel to a straight boundary with fluid (2). To maintain some similarity with the model jet parameters, let  $a_2 = 2a_1$ ,  $U = a_1$ .  $a_1$  and  $a_2$  are the speed of sound in fluids (1) and (2). Figure 7 shows the radiation pattern adopted by periodic wave fronts. In order to determine the form of the wave fronts radiated into region (2), it is necessary to calculate the refraction of the wave as it is transmitted across the boundary.

Referring to Figure 6a, consider the movement of the intersection of an incident wavefront with the fluid boundary during a time interval  $\tau$ . The displacement of the intersection has two components,

$$s = U\tau + \frac{a_1 \tau}{\sin \theta_1}$$

where  $U\tau$  is due to convection, at the velocity  $U$ , of the incident sound ray in the direction parallel to the boundary. The term  $a_1 \tau / \sin \theta_1$  is due to the acoustic propagation of the wavefront.

The trace distance  $s$  is also the distance moved by the intersection of the transmitted wave front along the boundary. Thus,

$$\frac{a_2 \tau}{\sin \theta_2} = U\tau + \frac{a_1 \tau}{\sin \theta_1},$$

and rearranging,

$$\sin \theta_2 = \frac{a_2 \sin \theta_1}{a_1 + U \sin \theta_1} \quad (1)$$

The transmitted waves of Figure 7 were constructed by applying Equation (1) at the wave/boundary intersections. It can be seen that a traveling spherical wave within medium (1) is radiated into the stationary medium (2) as an egg-shaped wave.

If  $\xi$  is the x-coordinate of an intersection of a wave front with the fluid boundary, the coordinates of the center of curvature of the transmitted wave are found to be

$$X = \frac{3\xi^2 - 1}{2\xi^3} ; \quad Y = 1 - \frac{1}{2} \left( \frac{2\xi^2 - 1}{\xi^2} \right)^{3/2} \quad (2)$$

as follows.

At time  $t$ , the radius of curvature of the incident wave, emitted at  $t = 0$ , is  $R_1 = a_1 t$ . Its incident angle  $\theta_1$  is given by

$$\sin \theta_1 = \frac{\xi - U t}{a_1 t} \quad (3)$$

Therefore, from Equation (1)

$$\sin \theta_2 = \frac{a_2 (\xi - U t)}{a_1^2 t + U (\xi - U t)}$$

and putting  $a_2 = 2a_1$ ,  $U = a_1$ ,

$$\sin \theta_2 = 2 \left( 1 - \frac{a_1 t}{\xi} \right) \quad (4)$$

Since the source is located at unit distance from the fluid boundary,

$$R_1^2 = a_1^2 t^2 = 1 + (\xi - U t)^2$$

and again putting  $U = a_1$

$$t = \frac{1 + \xi^2}{2 \xi a_1} \quad (5)$$

whence, substituting into (4)

$$\sin \theta_2 = 1 - \frac{1}{\xi^2} \quad (6)$$

Now from Figure 6b,

$$R_2 \Delta \theta_2 = \Delta \xi \cos \theta_2 \quad \text{where} \quad \Delta \theta_2 = \frac{d \theta_2}{d \xi} \cdot \Delta \xi \quad (7)$$

and from Equation (6)

$$\cos \theta_2 \cdot \frac{d \theta_2}{d \xi} = \frac{2}{\xi^3}$$

so that

$$R_2 = \cos^2 \theta \cdot \frac{\xi^3}{2} \quad .$$

where

$$\cos^2 \theta = 1 - \sin^2 \theta = \frac{1}{\xi^2} \left( 2 - \frac{1}{\xi^2} \right) \quad .$$

Thus,

$$R_2 = \xi - \frac{1}{2 \xi} \quad .$$

From Figure 6b, the coordinates of the center of curvature are:

$$X = \xi - R_2 \sin \theta_2$$

$$Y = 1 - R_1 \cos \theta_2$$

which leads to the result given as Equation 2.

The locus of the center of curvature is shown in Figure 7. It should be noted from Equation (1) that a condition for transmission is that  $|a_1 + U \sin \theta_1| < |a_2 \sin \theta_1|$ . If this condition is not satisfied then there is no solution for  $\theta_2$  and the wave is completely reflected. In fact, it can be shown that waves are transmitted only for  $\xi > 0.71$ .

If the point source were randomly intermittent in nature, both in amplitude and direction, then the transmitted wave pattern would consist of a series of short arcs having origins distributed along the locus shown in Figure 7.

Such a mechanism provides an explanation for the observed source locations in the jet shadowgraphs. To illustrate this point more fully, the results are applied to a simplified jet flow model. A source is assumed to exist at each shock/turbulence interaction location, and in the adjacent mixing region the flow properties are assumed constant, i.e., both convection velocity and speed of sound are constant between the sound source and the jet boundary where the waves cross it. The convection velocity is assumed constant, equal to 0.5 times nozzle velocity, for all three locations, and an equivalent speed of sound is calculated for each from total jet momentum considerations. Assuming conservation of momentum along the jet, the momentum of the mixing region at any axial station is obtained from the dimensions of the laminar core, which retains the nozzle flow conditions. Then using an exponential velocity profile of the form

$$v = V e^{-(r - r_c)^2}$$

for the mixing region, an equivalent mean density,  $\bar{\rho}$ , is derived from the assumed relationship:-

$$\text{local mixing region momentum} = (\text{nozzle momentum minus local laminar core momentum})$$

$$= \bar{\rho} \int_{r_c}^{r_b} v^2 2\pi r \, dr$$

where  $r$  = radial coordinate,  $r_c$  = radius of laminar core and  $r_b$  = radius of outer jet boundary.  $\bar{\rho}$  leads to an equivalent mean temperature which in turn yields a mean speed of sound. For the first three shock intersection positions, the equivalent values of the speed of sound were calculated to be 740, 790, and 900 ft./sec. The convection velocity was based on a nozzle Mach number of  $M_E = 1.47$  and is therefore equal to 785 ft./sec.

Approximate apparent source loci obtained from these parameters are shown in Figure 5, and clearly show reasonable agreement with the observed sources. The errors could well be explained as a result of the crude jet-flow model used but the agreement seems sufficient to justify linking the observed sources with the specified shock turbulence intersections.



#### 4.0 CONCLUSIONS AND RECOMMENDATIONS

A series of experiments has been performed to investigate the effects of varying the film position and the focussing effects of lenses on the shadowgraphs of the flow and acoustic field of a small supersonic jet. Some of the results are presented as plates 1 through 9. The experiments were of a preliminary nature but have shown that film location is an important variable for consideration during the design of shadowgraph experiments. The only significant focussing effects produced by diverging and converging lenses were to either magnify or diminish the size of the image.

For a cold jet the main conclusions are as follows:

1. Small film distances are desirable for general observation of the jet flow structure, especially the shock formation. At increasing distances, the shock boundaries become less clearly defined and the "cylindrical lens" action of the flow distorts the flow dimensions.
2. The shock structure is only clearly visible within the confines of the laminar core. The shock fronts which exist within turbulent flow are apparently too dispersed to form a clear shadowgraph image. Shadowgraphy could therefore provide a convenient method for determining laminar core boundaries within non-luminous supersonic jets.
3. The turbulence scale shows an apparent increase with increased film distance. The effect is probably due to the fact that larger eddies have greater effective focal lengths. It will also be true that weaker eddies are focussed at greater distances.
4. Up to a certain limit, which in this case was between 50 and 100 centimeters, increasing the film distance clarifies the acoustic field. This is basically due to the magnification effects, but in addition to broadening the apparent width of the wave fronts, an increase in distance does reveal waves which are not visible at shorter distances. This is probably due to a similar effect to that of (3) above, i.e., weaker waves focus light at greater distances from the flow.
5. The predominant visible acoustic radiation from the observed region of the jet, namely the first 10 diameters or so of the exhaust stream, takes two basic forms; a highly directional radiation from a region near the nozzle which is approximately two diameters long, and multidirectional radiation from a series of highly localized regions associated with the shock structure.

6. The directional radiation shows some characteristics of Mach waves, but the associated eddy convection velocities appear to be much closer to the nozzle exhaust velocity than has previously been suggested.
7. The apparent sources of the multidirectional radiation patterns are located downstream and outwards from the points where the flow compression shocks penetrate the supersonic turbulent cone. However, it is shown from a consideration of wave propagation and refraction that the radiation probably originates from those particular shock/turbulence intersection points.

The results of these experiments suggest the following guidelines for additional research:

1. If the directional radiation from the region near the nozzle is of the form of Mach waves, the origin of the very high velocities of the generating eddies is mysterious. An alternative explanation is that this radiation is more closely related to the shock/turbulence noise than to Mach waves. It could well be radiated by the interactions of flow disturbances generated upstream of the nozzle, or within the nozzle boundary layer, with standing shocks in the nozzle expansion chamber. Additional study, using higher velocity jets, is required to resolve this problem.
2. Further work is required to substantiate the proposition that the multidirectional radiation is generated by the interaction of supersonically convected turbulence with the standing compression shock in the exhaust stream. A more accurate model is required for the analytical prediction of the propagation and refraction effects and further experimental work could include a shadowgraph study of jets with a variety of standing shock configurations. It should be noted that jet temperature should have a significant effect upon apparent source location. Also these locations could probably be measured more accurately by using greater film distance to make use of the enhanced image of the radiation. This would probably require the use of a more intense spark (or faster film) and larger sheets of film to cover adequate areas.

## REFERENCES

1. Lowson, M. V., "Shadowgraph Experiments in the Marshall Space Flight Center Jet Flow Facilities", Wyle Laboratories Research Staff Technical Memorandum 66-15, April 1966.
2. Ames Research Staff, "Equations, Tables and Charts for Compressible Flow", NACA Report 1135, 1953.
3. Phillips, O. M., "On the Generation of Sound by Supersonic Turbulent Shear Layers", J. Fluid Mech., Volume 9, 1960.
4. Ffowcs Williams, J. E., "The Noise From Turbulence Convected at High Speed", Proc. Roy. Soc., Volume A 255, 1963, pp. 469-503.
5. Eldred, K. M., "Suppression of Jet Noise with Emphasis on the Near Field", ASD-TDR-62-578, 1963.
6. Anderson, R. A., and Johns, F. R., "Nondimensional Characteristics of Free and Deflected Supersonic Jets Exhausting into Quiescent Air", NADC-ED-5401, March 1954.

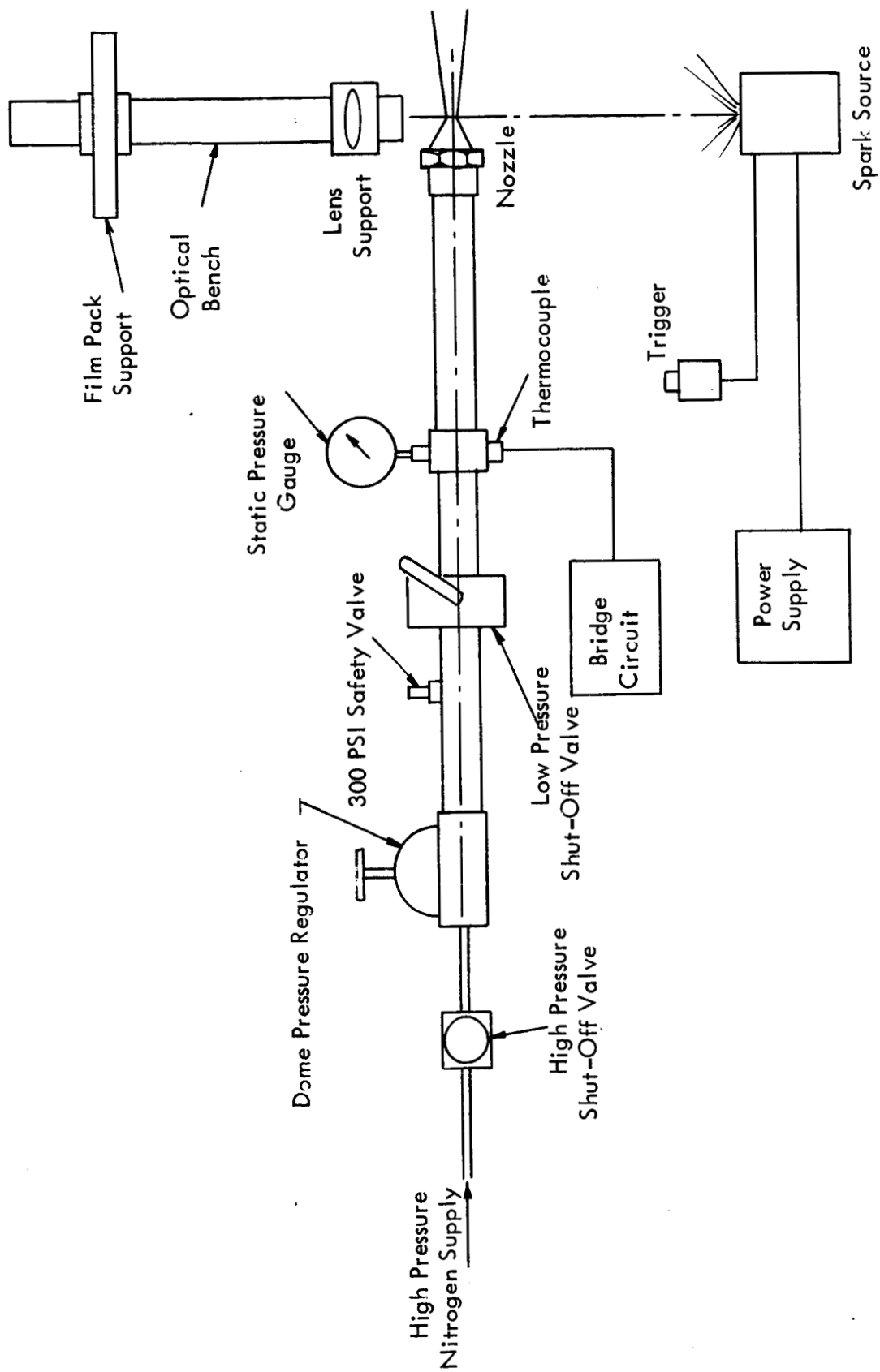


Figure 1: Experimental Apparatus.

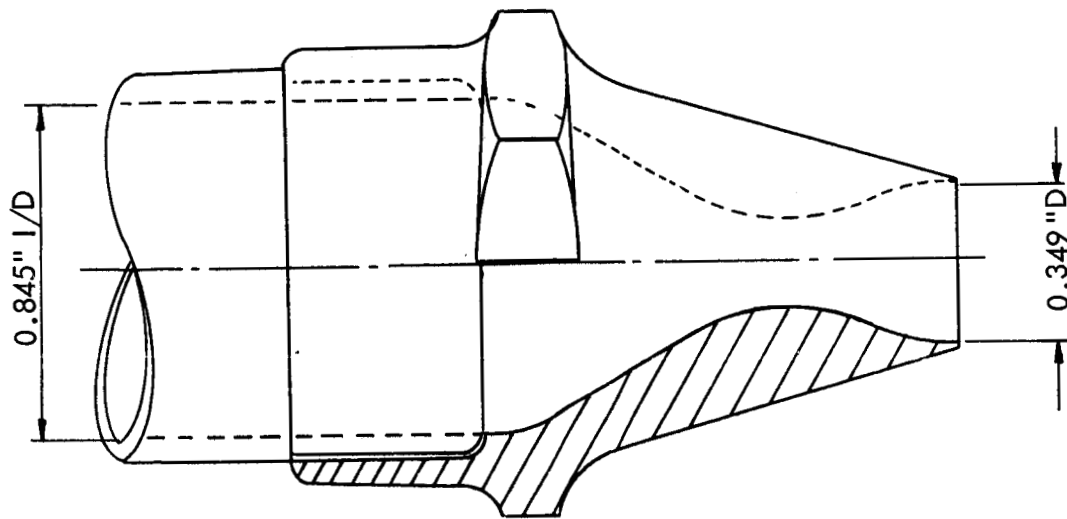


Figure 2: Model Jet - Convergent/Divergent Nozzle.

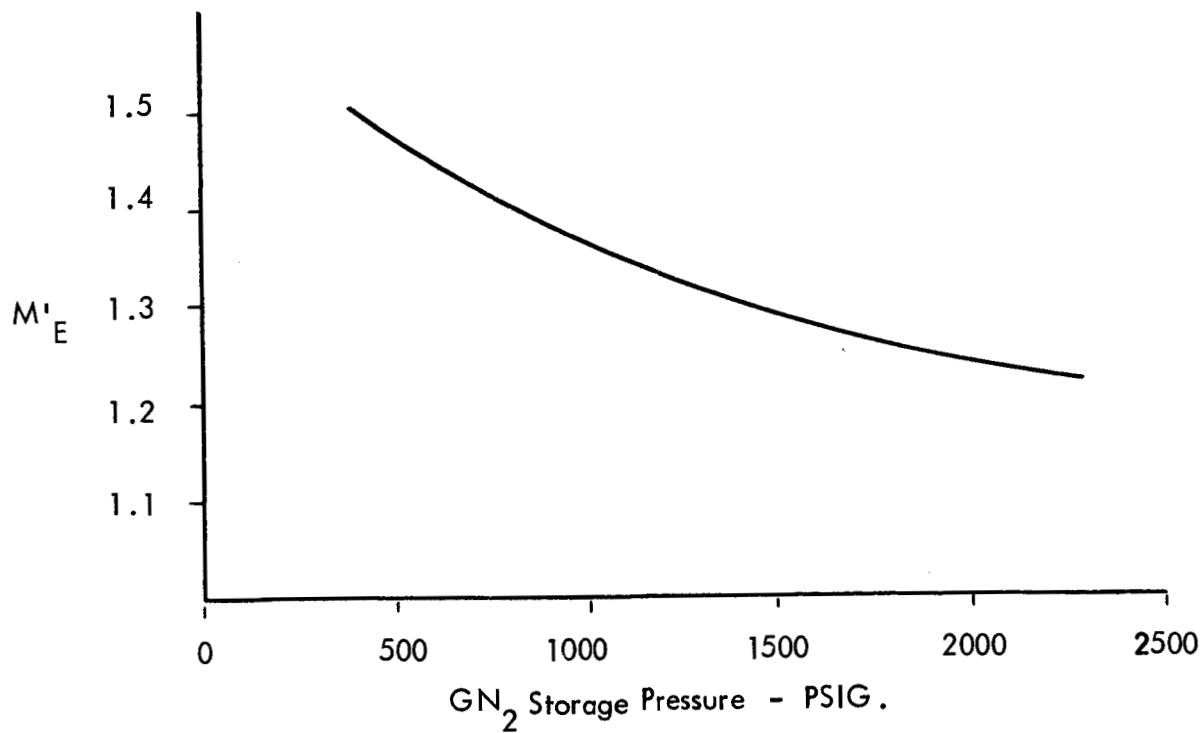


Figure 3: Variation Of Nozzle Exit Velocity (Expressed As Mach Number Relative To Ambient Speed of Sound) With Nitrogen Storage Pressure.

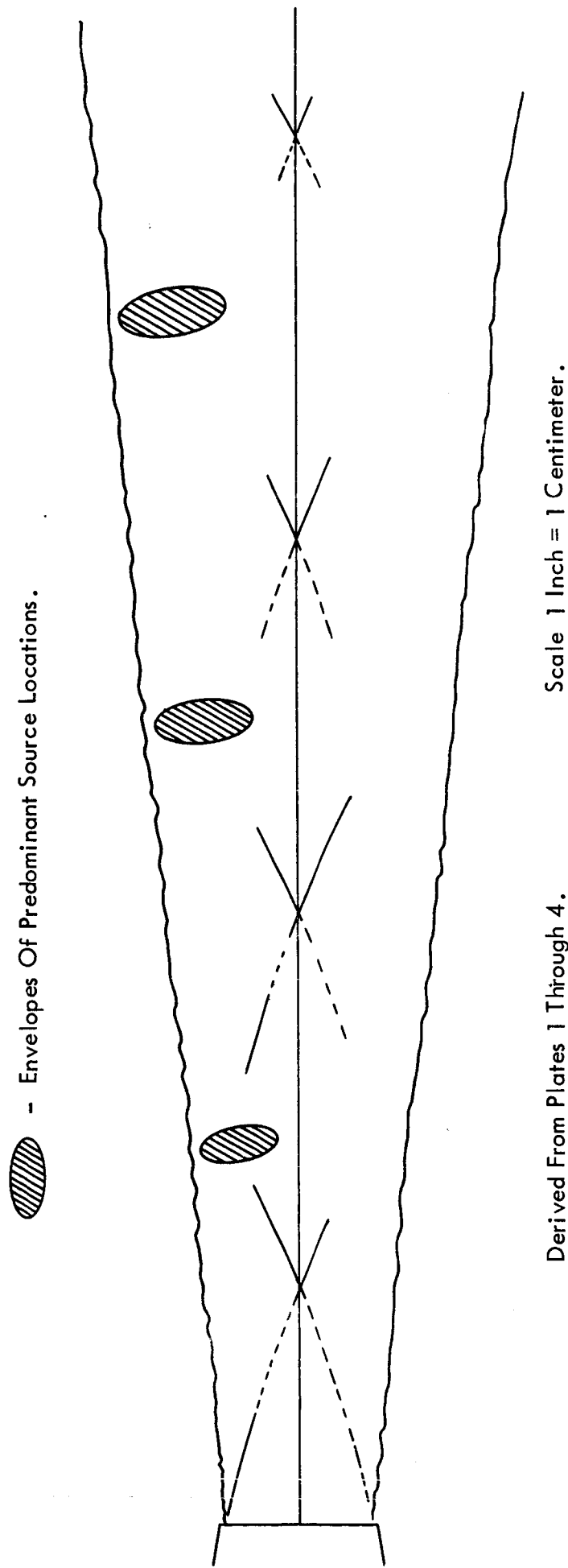
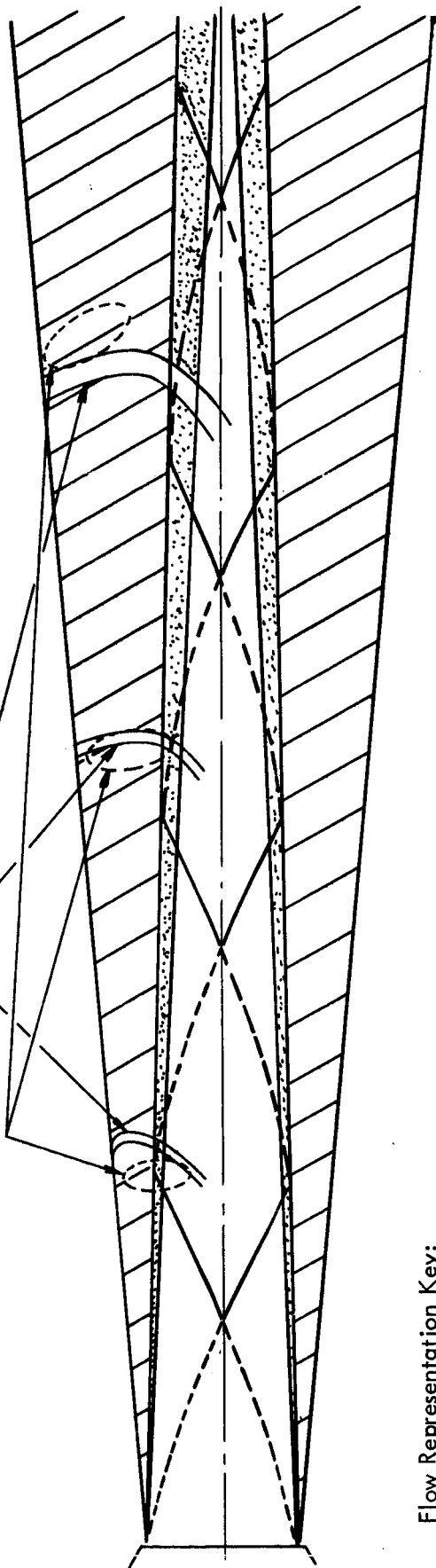


Figure 4: Regions Of Apparent Locations Of Multi-Directional Sound Sources.

# Approximate Envelopes of Apparent Source Locations

Theoretical

Measured



Scale 1" = 1 Centimeter

## Flow Representation Key:




-  Supersonic - Laminar (Boundary After Eldred - Reference 5)
-  Supersonic - Turbulent (Boundary After Anderson and Johns - (Reference 6)
-  Subsonic - Turbulent

Figure 5: Idealized Representation of Flow Structure Showing Acoustic Source Location

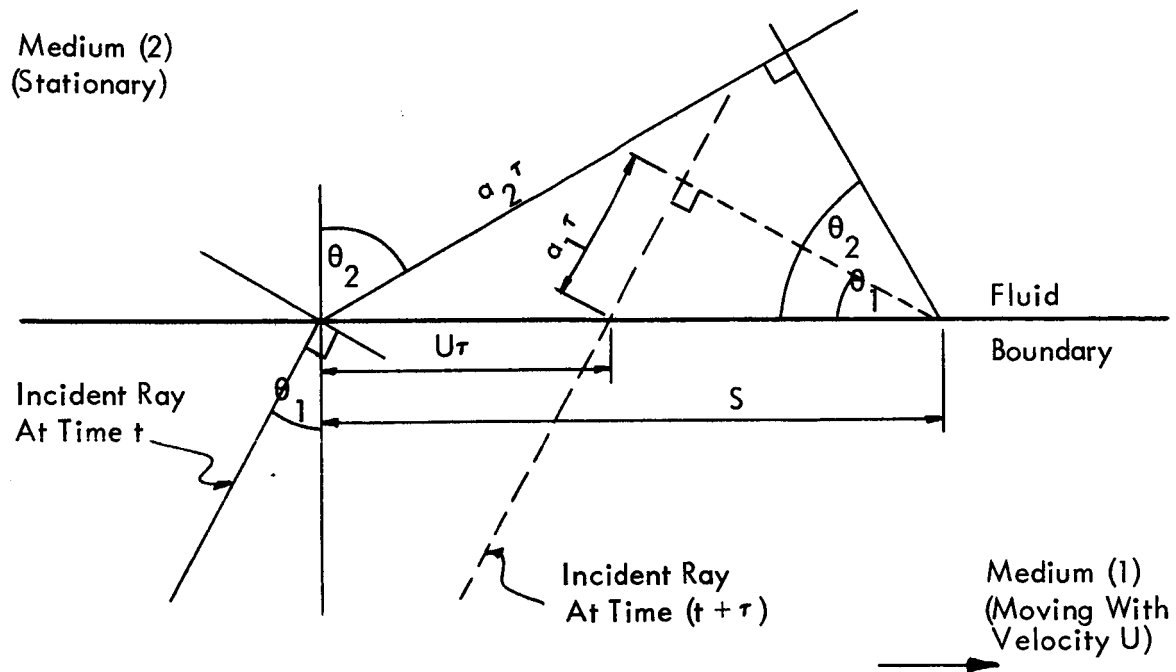


Figure 6a: Sound Ray Refraction.

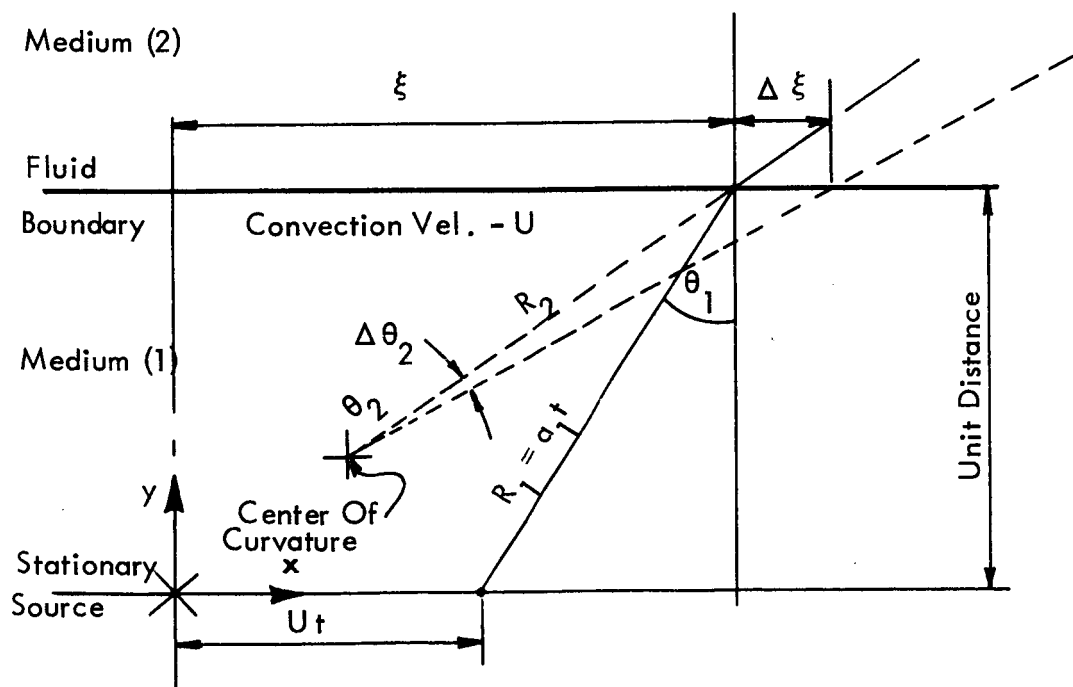


Figure 6b: Center Of Curvature Of Transmitted Waves.



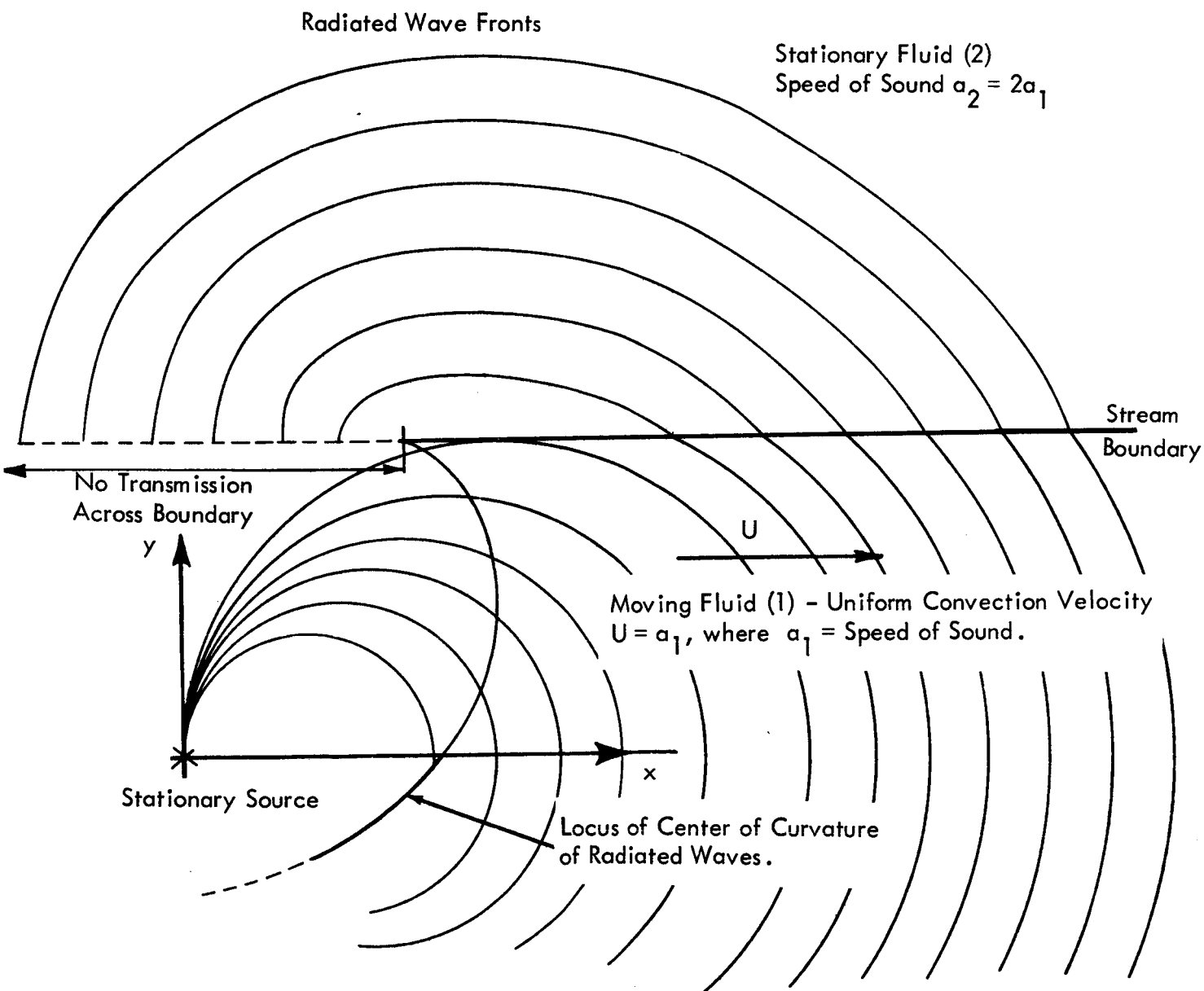


Figure 7: Wave Propagation and Radiation From a Stationary Simple Source Immersed at Unit Depth in a Fluid Moving With Sonic Velocity

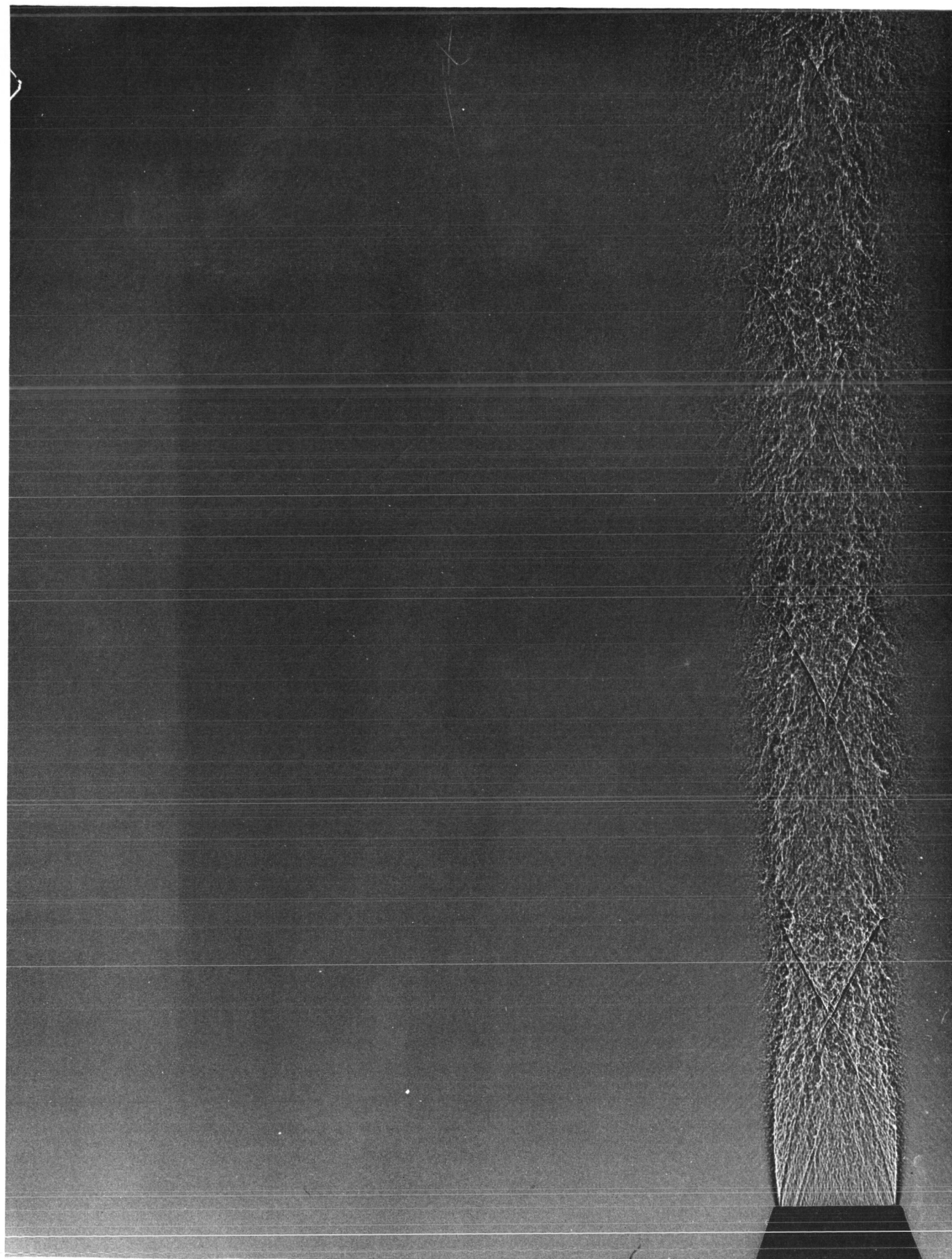


Plate 1. Film Distance - 5 Centimeters

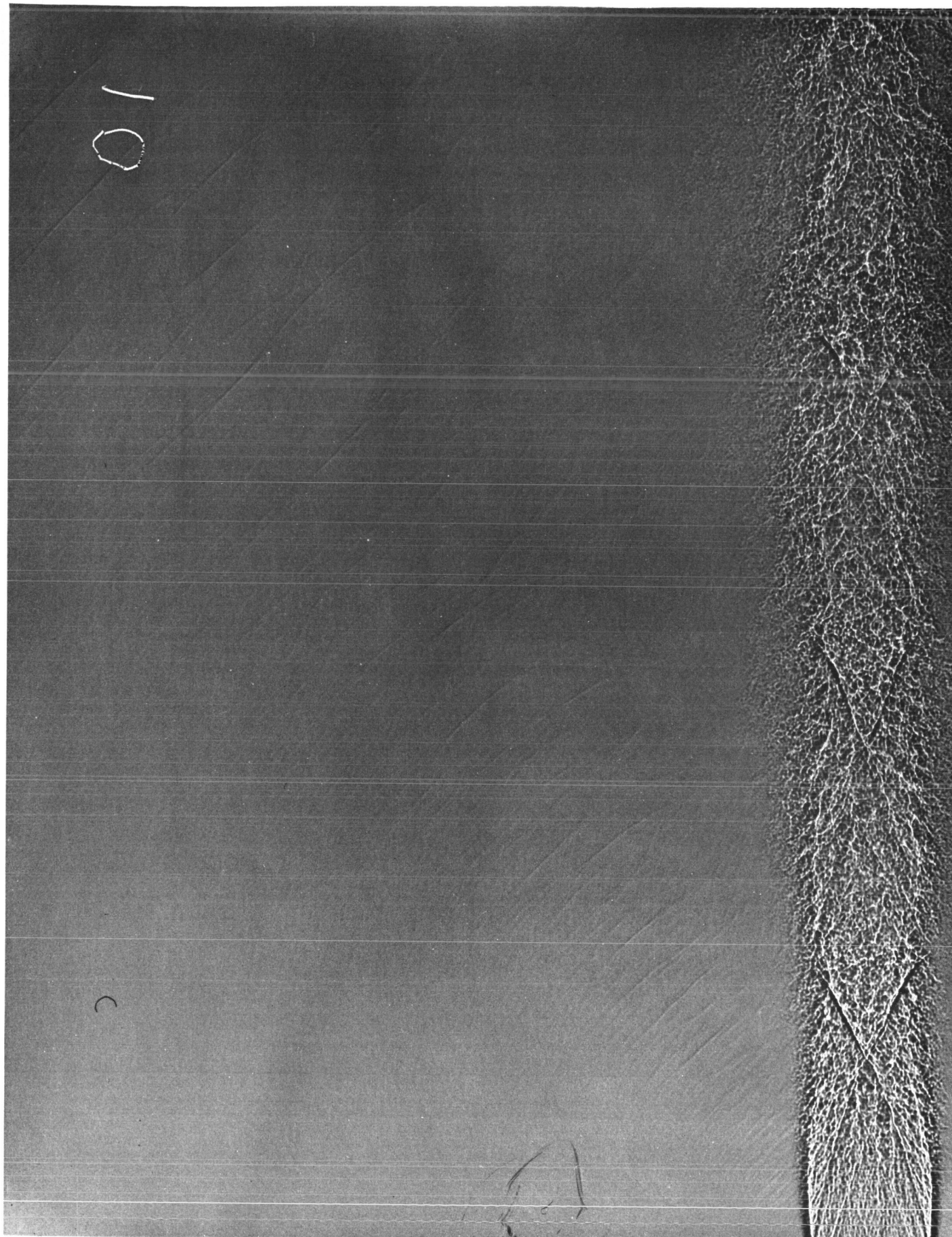


Plate 2. Film Distance - 10 Centimeters



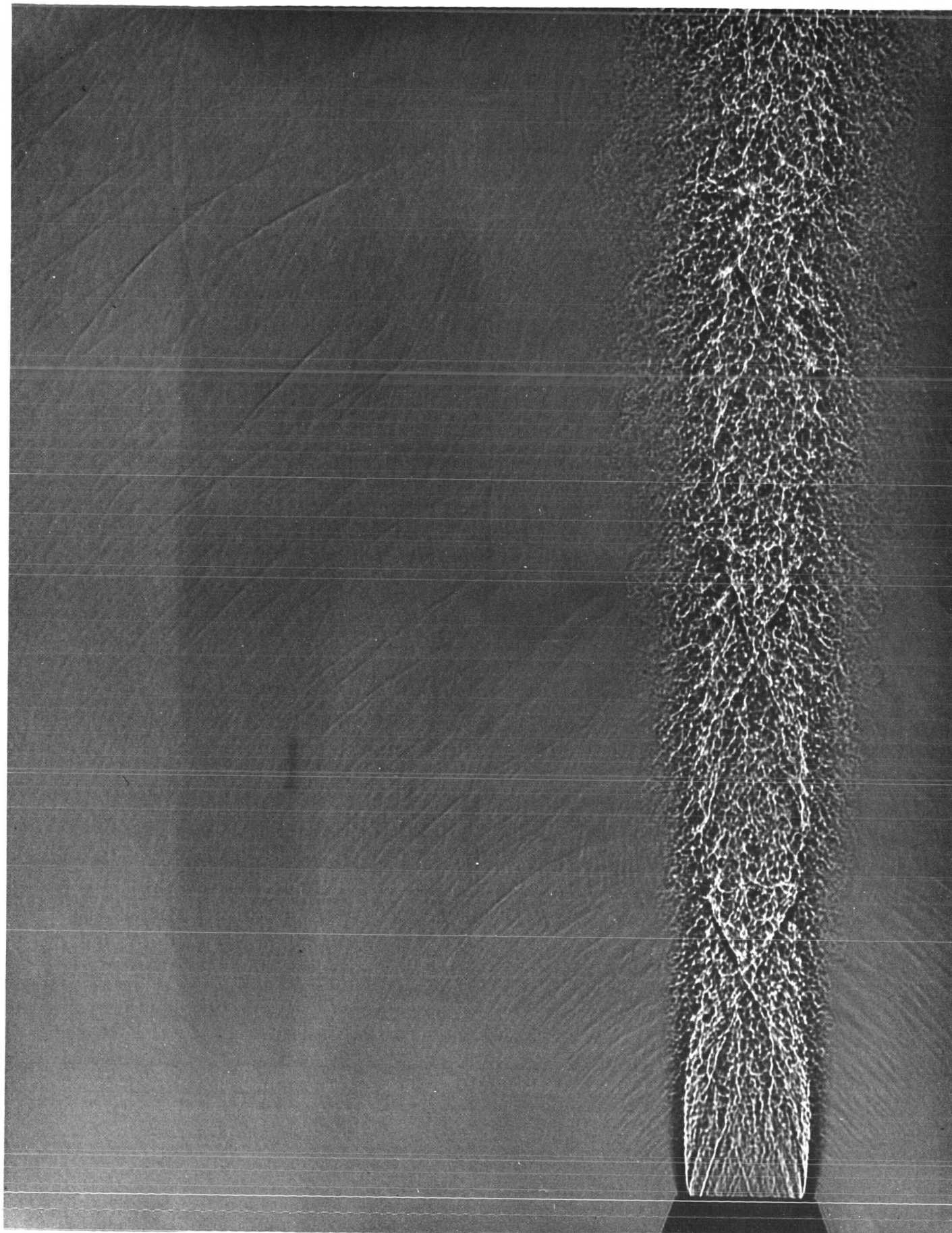


Plate 3. Film Distance - 20 Centimeters

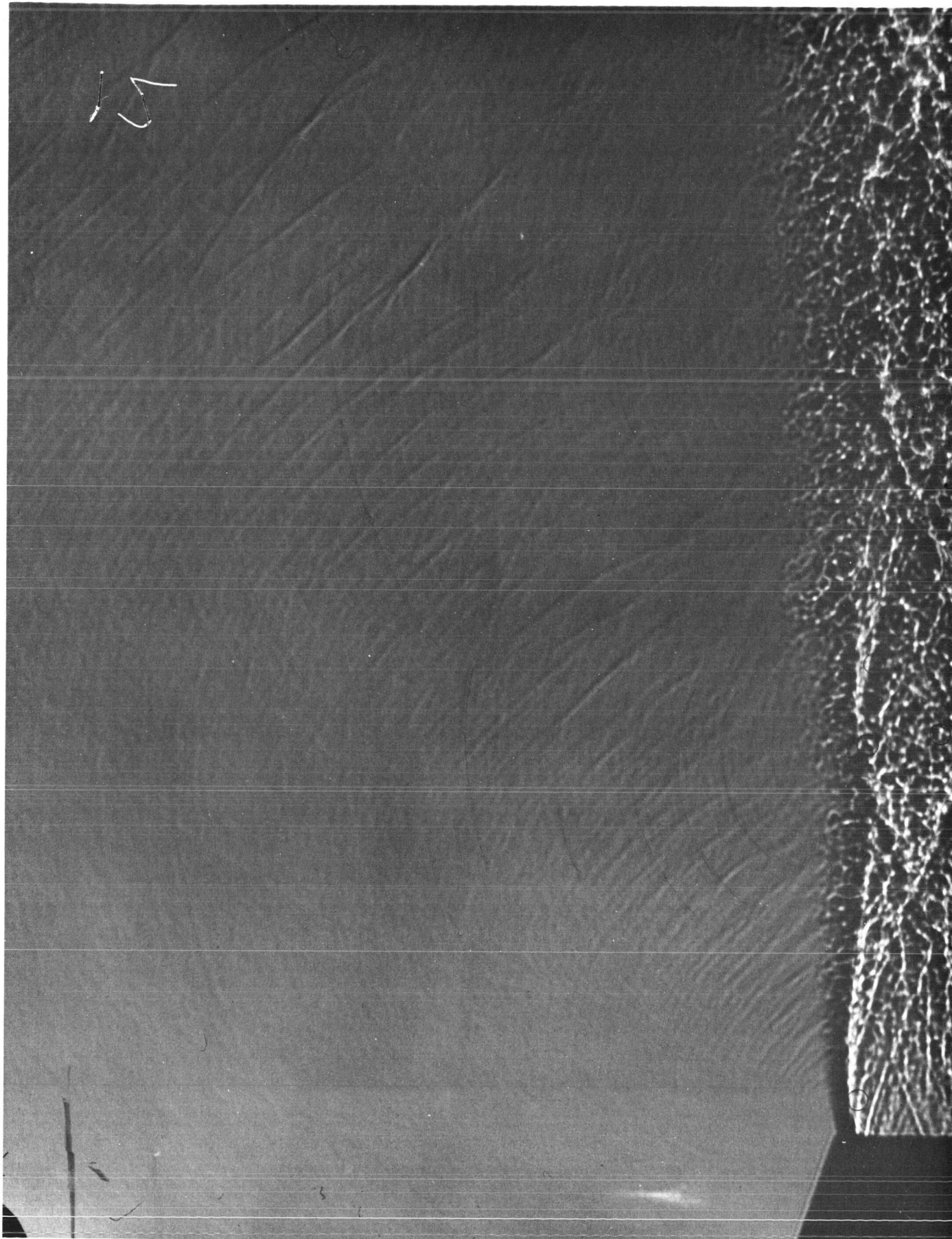


Plate 4. Film Distance - 50 Centimeters



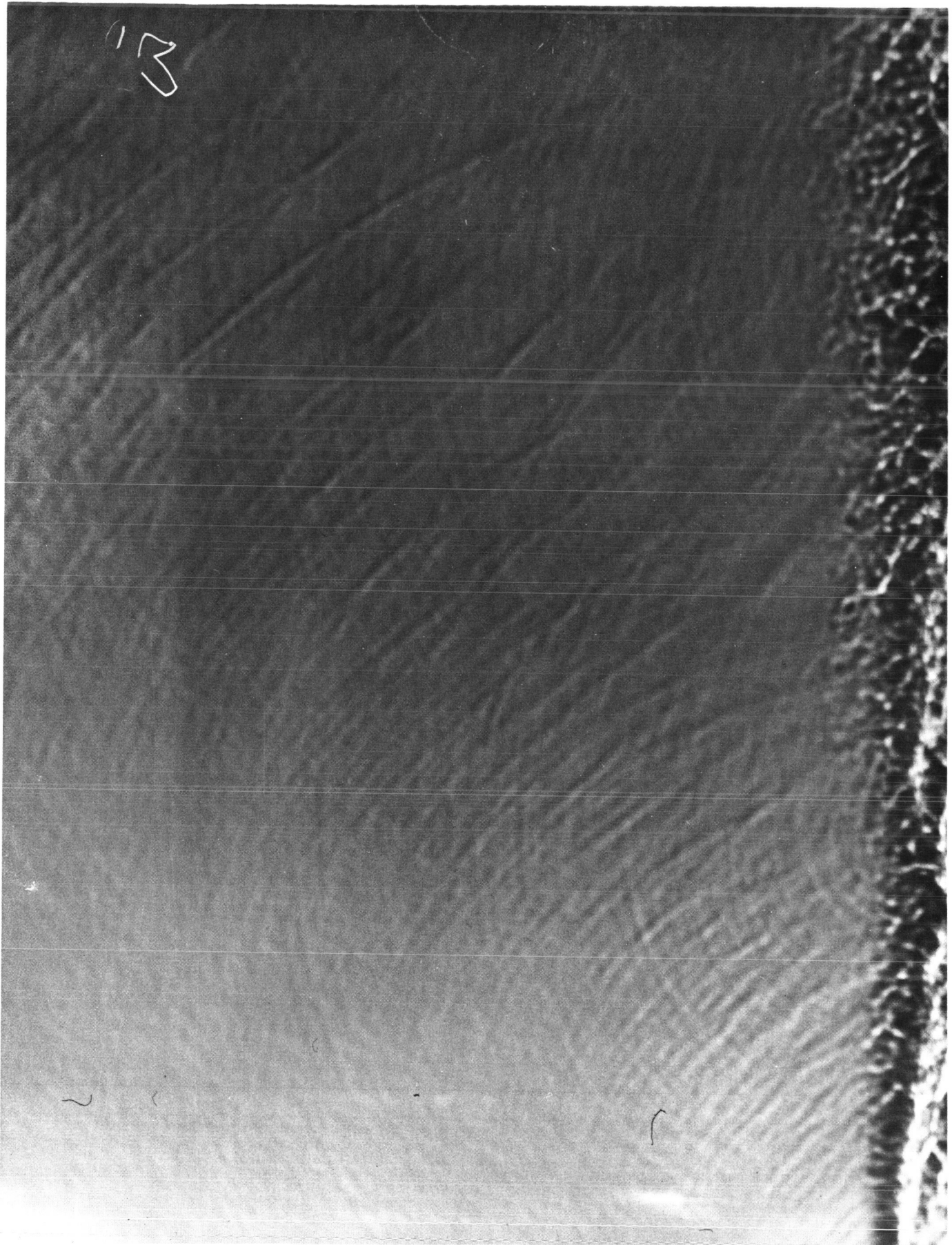


Plate 5. Film Distance - 100 Centimeters

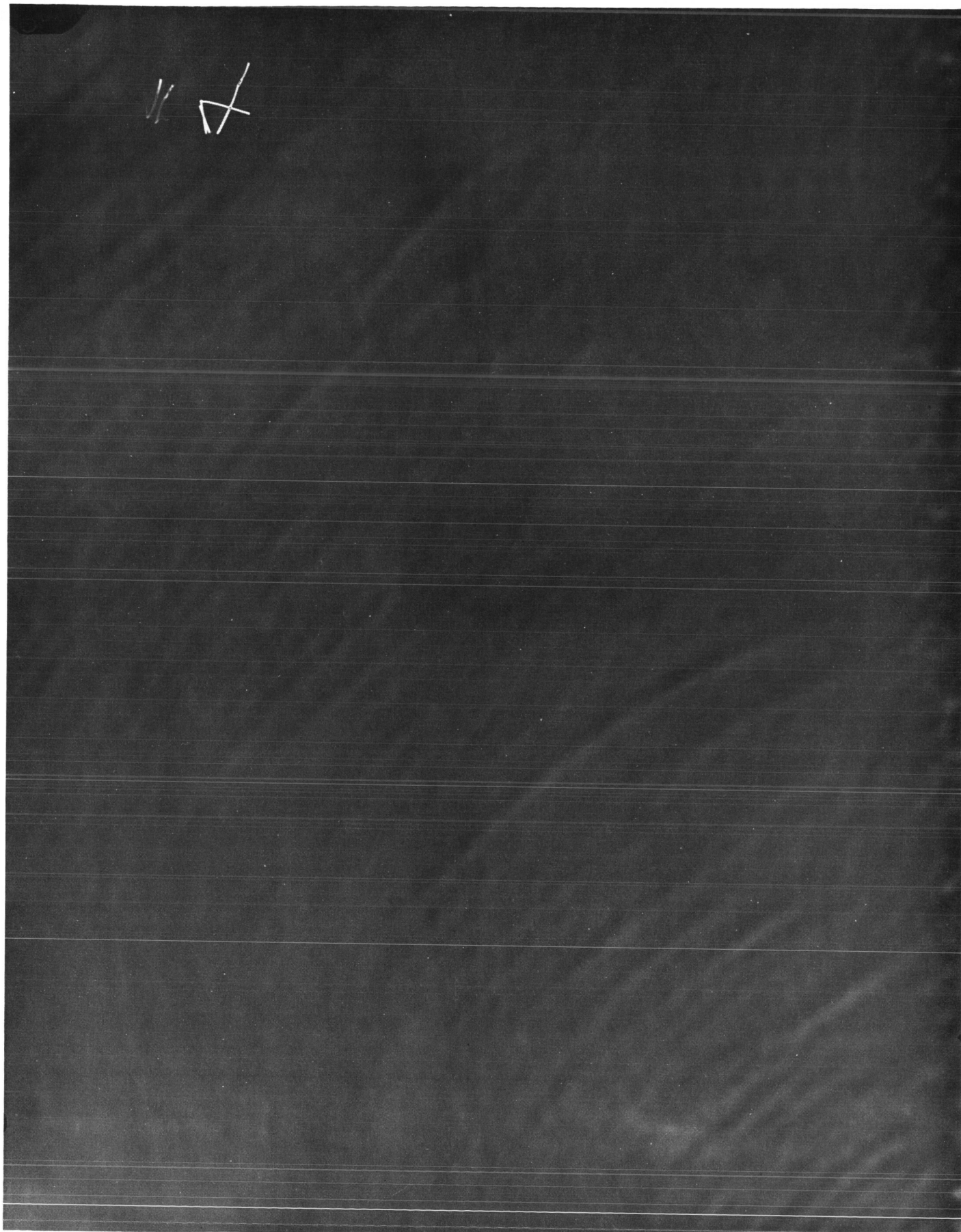


Plate 6. Film Distance - 200 Centimeters



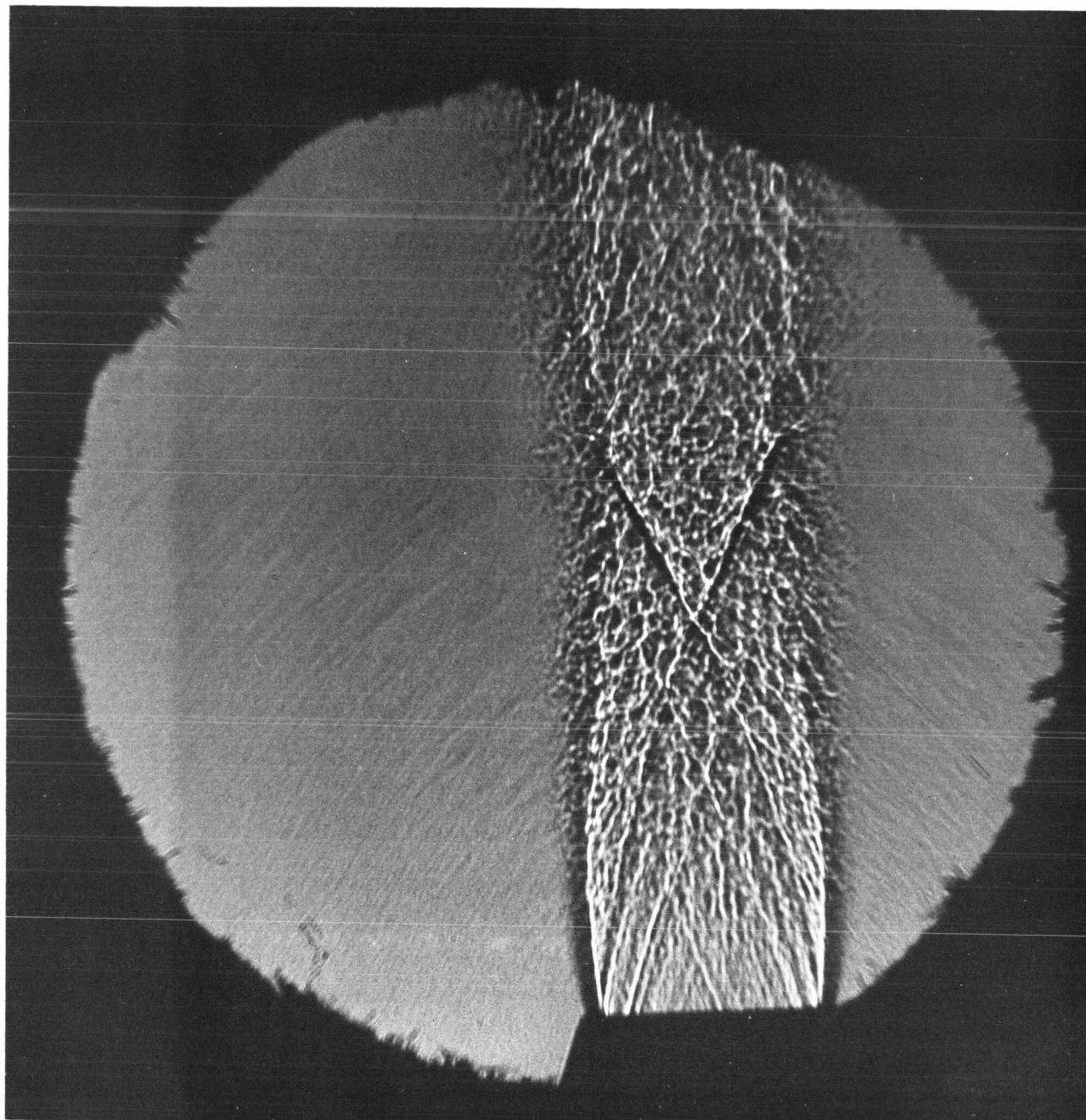


Plate 7. Film Distance - 20 Centimeters - 20 Centimeters Focal Length  
Diverging Lens at 10 Centimeters



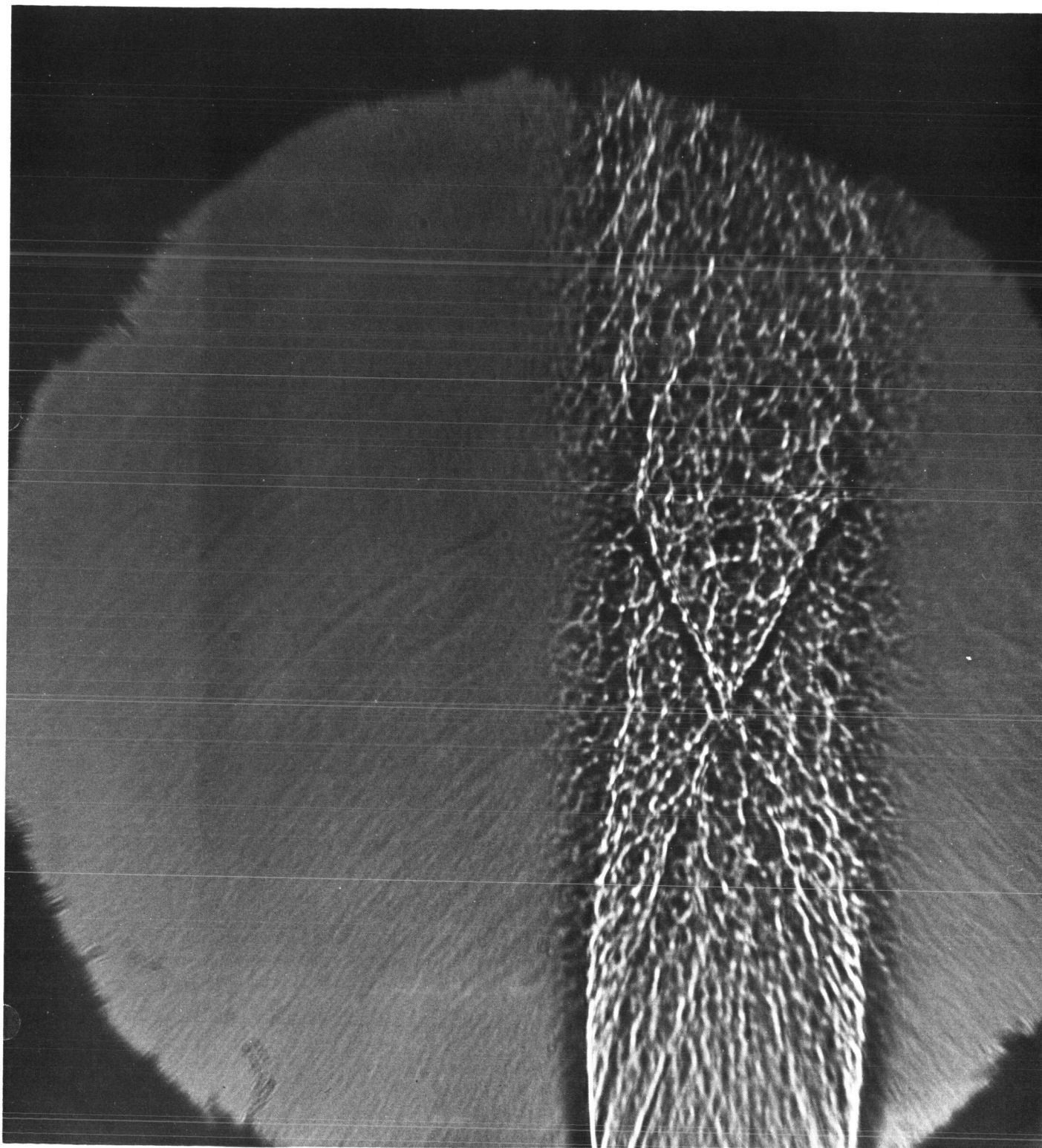


Plate 8. Film Distance - 30 Centimeters - 20 Centimeters Focal Length  
Diverging Lens at 10 Centimeters

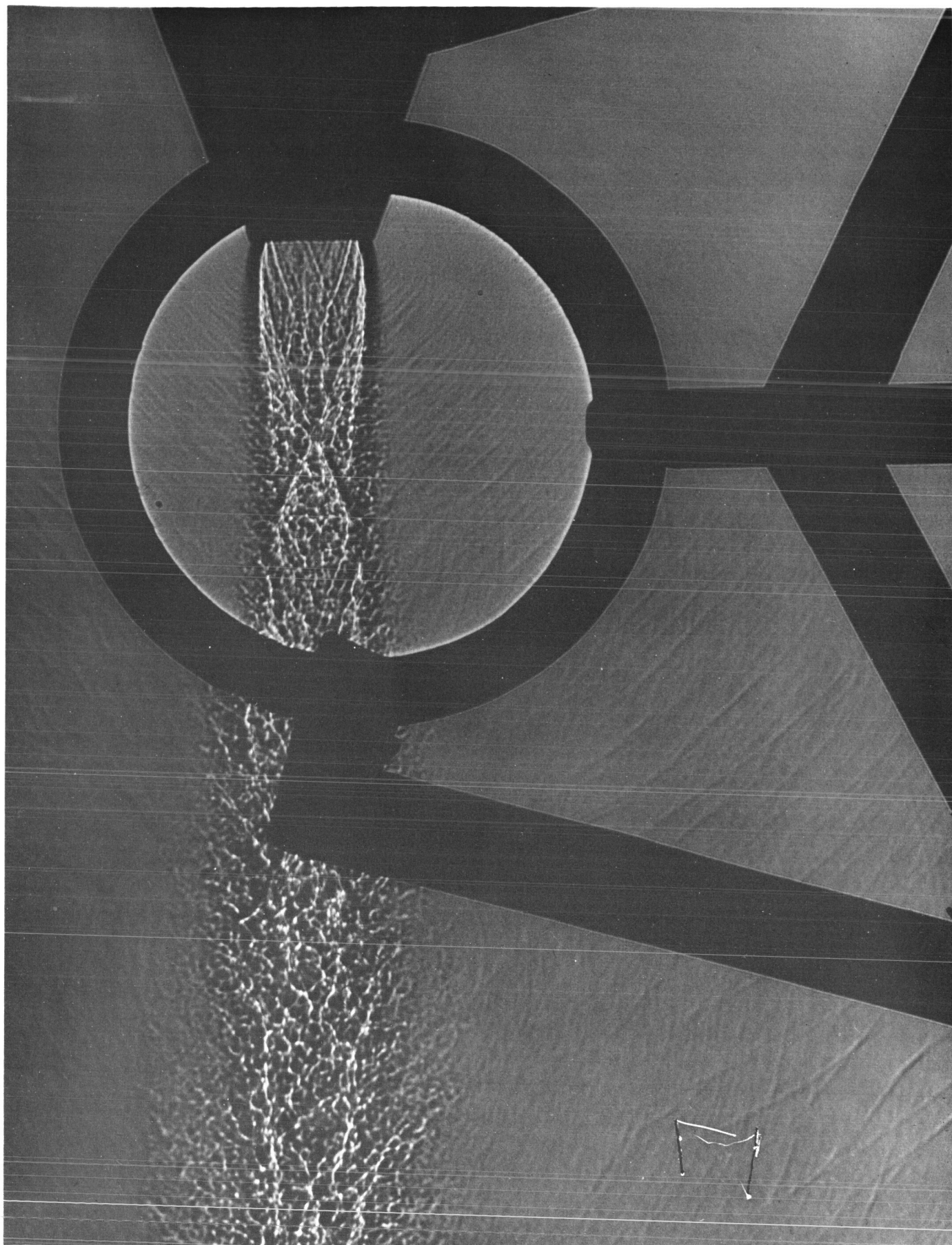


Plate 9. Film Distance - 40 Centimeters - 100 Centimeters Focal Length  
Converging Lens at 20 Centimeters